Journal of Magnetism and Magnetic Materials 634 (2025) 173540

Contents lists available at ScienceDirect

Journal of Magnetism and Magnetic Materials

journal homepage: www.elsevier.com/locate/jmmm

Research article

Reversal of the internal magnetization of one-dimensional and two-dimensional domain walls

Sukhvinder Singh *, Haibin Gao, Uwe Hartmann

Institute of Experimental Physics, Saarland University, 66123, Saarbrücken, Germany

ARTICLE INFO

Keywords:
Permalloy
Magnetic domains
Domain walls
Magnetic force microscopy

ABSTRACT

Investigations of the internal structures of domain walls have attracted great attention in magnetism for potential applications such as sensors, racetrack memories and spin-wave-based logic operations. In this work, we investigated the role of vortices and antivortices in the transformations of the internal magnetization configuration of one-dimensional and two-dimensional domain walls in Permalloy thin films. The magnetization reversal of the one-dimensional domain walls proceeds with in-plane rotations of their magnetizations. In contrast, the magnetization reversal of the two-dimensional domain walls proceeds with in-plane rotations of their magnetizations at the surfaces and out-of-plane rotations of their magnetizations in the interiors of the walls. Both types of domain walls reverse their internal magnetizations by displacing a resulting single vortex along their wall axes. This displacement proceeds via the nucleation and annihilation of vortices and antivortices inside the walls.

1. Introduction

The control and modulation of the internal magnetization configurations of domain walls is a focus of extensive research in magnetism [1–10]. The reversal of the bi-stable orientation of the internal magnetization of domain walls has been purposed for magnetic data storage [2,3,10] and sensor [5] applications. Controlled internal configurations of domain walls are required for a reliable operation of racetrack memories [4,6,7,11,12] and spin-wave-based logic operation circuits [13–16]. Moreover, the internal configurations of domain walls within applied external fields [9,17] and current pulses [18] are investigated for topological spintronic applications [17,19]. The internal magnetization configurations of domain walls depend on the thickness [20] and magnetic anisotropy [21–23] of the constituting material. In a soft magnetic material such as Permalloy (Py), the magnetization configurations of domain walls change from one-dimensional to two-dimensional at ~100 nm with an increase of the film thickness [20,24]. In a Py film of a thickness of $\lesssim$ 20 nm, one-dimensional symmetric Néel walls (SNWs) exist [20,24]. The magnetization inside the SNWs is oriented only in the plane of the film. For an intermediate film thickness, i.e., from approximately 20 to 100 nm, cross-tie walls (CTWs) exist. These are composed of oppositely oriented one-dimensional SNW segments separated by alternate vortices and antivortices [20,25,26]. In these walls, the oppositely oriented one-dimensional SNW segments are arranged in a cross-tie configuration [20,25,26]. In thicker films with a thickness $\gtrsim$100 nm, two-dimensional asymmetric domain walls (ADWs) exist [20]. The ADWs possess both in-plane and out-of-plane orientations of magnetization. The ADWs minimize their stray field by turning their magnetization in the plane of the film at the surfaces and out of the plane of the film in their interiors [20,27,28]. The near-surface magnetization regions inside the walls with an in-plane magnetization are called Néel caps (NCs), and the magnetization regions in the interiors of the walls with an out-of-plane magnetization are called Bloch cores of the walls [20,27,28]. The ADWs are further classified into asymmetric Néel walls (ANWs) and asymmetric Bloch walls (ABWs) depending on their "S-" and "C-type" cross-sectional magnetization configurations, respectively [20,24]. In the ANWs, the upper and lower NCs are formed on the left and right sides of the Bloch cores or vice-versa [20]. However, in the ABWs, both the upper and lower NCs are formed on the same side of the Bloch cores [20]. In our previous studies, we determined that perpendicular anisotropy splits the Bloch cores inside the ANWs into alternately upwards- and downwards-tilted magnetization segments [21]. However, the Bloch cores inside the ABWs do not split due to the presence of a vortex-like structure in the cross-sections of the ABWs [21].

The internal magnetizations of the domain walls also transform within an applied magnetic field [8,9,20,24,29,30]. These transformations proceed with the nucleation of various types of transition structures (TSs) inside the walls; TSs separate the domain wall segments of different magnetization configurations [26,30–39]. In one-dimensional

* Correspondence to: Fraunhofer Institute for Silicon Technology, Itzehoe 25524, Germany.
E-mail address: sukhvinder.singh@isit.fraunhofer.de (S. Singh).

https://doi.org/10.1016/j.jmmm.2025.173540
Received 4 May 2025; Received in revised form 23 September 2025; Accepted 23 September 2025
Available online 27 September 2025

domain walls, vortices and antivortices are formed as TSs [25,26,40]. However, in two-dimensional domain walls, different combinations of vortices and antivortices at the surfaces and magnetic singularities (i.e., the Bloch points (BPs)) [9,39,41–45] in the interiors of the walls form various types of complex three-dimensional TSs [35,36,39,45–47]. The micromagnetic simulations [26,31–33,35,36,38,39,41,43,47,48] and other theoretical work [20,49,50] on the configurations of the different types of TSs as well as their observed behaviors inside the domain walls by different experimental techniques [9,37,42,44,46] have been reported in the literature. Nguyen et al. [4] investigated the internal structure of two-dimensional domain walls in Py stripe structures and found out that these walls can be moved with an external magnetic field of about 1 mT. Zverev et al. [31,32,39,40] and Redjdal et al. [36,47] described the detailed configurations of various types of the TSs inside the ABWs and ANWs in Py films. However, despite the vast knowledge of the TSs and various types of domain walls, the role of TSs in the transformations of the internal magnetizations of two-dimensional domain walls has not been investigated in detail.

In this study, the role of vortices and antivortices as TSs in the reversal of the internal magnetizations of one-dimensional and two-dimensional domain walls is investigated. Py patterns with lateral dimensions of 2.3×6.7 μm^2 and thicknesses of 40 and 130 nm were fabricated to investigate the configuration transformations inside one-dimensional and two-dimensional domain walls, respectively. To investigate the magnetizations inside a single domain wall, the short-axis magnetization reversals of these elongated rectangular structures were analyzed using Magnetic Force Microscopy (MFM). The short axis reversal favors the formation of a single domain wall perpendicular to the direction of the applied magnetic field. Additionally, the corresponding micromagnetic simulations were performed to understand the three-dimensional magnetization transformations inside the domain walls.

2. Experimental and micromagnetic simulation details

The micropatterned Py ($Ni_{80}Fe_{20}$) films were fabricated using electron-beam lithography (EBL) and DC magnetron sputtering techniques. First, a thin layer of a positive poly methyl methacrylate resist was spun onto the silicon substrates, and then the resist layer was patterned and developed using EBL. Thereafter, Py films with thicknesses of 40 and 130 nm were deposited at 2.0 μbar Argon pressure with a constant sputter rate of 18 nm/min. After the deposition, a lift-off process was performed in an acetone bath, and the samples were cleaned with de-ionized water. No protective capping layer was deposited on the samples.

Magnetic imaging of the samples was performed with a Bruker Multimode 8 MFM using Olympus AC240TS cantilevers coated with a 30 nm thick CoCr layer [51]. For micromagnetic calculations, the Object-Oriented MicroMagnetic Framework (OOMMF) software [52] with cubic cells of $20\times20\times10$ nm^3 size were used. The saturation magnetization of $M_s = 860$ kA/m, an exchange constant of $A = 13\times10^{-12}$ J/m, and a gyromagnetic ratio of $\gamma = 2.21 \times 10^5$ m/As were assumed in the simulations. To perform the static simulations, a damping parameter of $\alpha = 0.5$ was applied. The convergence criterion $|\boldsymbol{M} \times \boldsymbol{H}|/M_s^2 \leq 1 \times 10^{-5}$ as a torque-minimization condition was employed in the calculations [53]. The simulations were performed without considering any influence of the temperature on the magnetization processes [54].

3. Reversal of the internal magnetization of one-dimensional domain walls

The domain configurations investigated by MFM at various applied fields are shown in Fig. 1. The corresponding simulated images are shown in Fig. 2. The sample is initially saturated along the +y direction (directions defined in Fig. 2). With a decrease in the applied field, the domain walls formed along the long edges of the sample (not shown in the results) join to form a single domain wall parallel to the x axis, as shown in Figs. 1(a) and 2(a). This domain wall is connected to two domain wall junctions on its ends [55–57]. In Fig. 1(a), this domain wall forms a bipolar contrast, changing its appearance from bright-brown to dark-brown colored along the +y direction. In the simulated image Fig. 2(a), the contrast of this domain wall changes from orange to green along the +y direction. Opposite magnetic charges inside the two halves of the wall, which are produced by an in-plane rotation of the magnetization inside the domain wall, produce a bipolar contrast in the MFM scan [20,58]. A continuous contrast of this domain wall along its length indicates the absence of any TS inside the wall. In Fig. 1(a), the domain wall forming the upper trapezoidal-shaped domain (the domain formed with the upper long edge of the sample) changes its contrast at the left domain wall junction. The change in the domain wall contrast along the broken line is visible in Fig. 1(a). The contrast of this domain wall remains unchanged at the right domain wall junction. The reversal of the domain wall contrast at the left wall junction indicates the presence of a vortex on the left domain wall junction, indicated by a black arrow in Fig. 1(a). Simplified schematics for the configurations of a domain wall junction with and without a vortex are shown in Fig. 3. In these images, it is shown that a vortex may or may not form at the wall junction knot depending on the orientations of the magnetization inside the domains and domain walls around the knot [57]. They are formed to minimize the total energy of the magnetic system. Depending on the applied external field, the domain wall junctions with and without vortices form and arrange within the domain configurations to minimize the magnetic stray field energy. The domain wall formed parallel to the x axis in Fig. 1(a) is a SNW with a vortex formed at its left end. This is also confirmed in Fig. 2(a) with the magnetization inside the SNW oriented along the +y direction. A schematic illustration of such a SNW formed at high positive field is shown in Fig. 4(a). The angle of this SNW increases with a decrease in the applied external field, because the magnetization inside the adjacent domains relaxes more along the sample edges. This, in turn, increases the magnetic charges inside the domain wall, thereby decreasing the stability of the domain wall [20]. On further decreasing the applied field, i.e., at +1.7 mT (Fig. 1(b)), the SNW stabilizes with the nucleation of vortex-antivortex pairs (VAVPs) as TSs. Locations of a vortex and an antivortex in one of the VAVPs are indicated with dashed arrows in Fig. 1(b). The nucleation of VAVPs transforms the SNW into a CTW [25,26]. In a 40 nm thick Py film, the SNW with the wall angle $\gtrsim$100° transforms into a cross-tie pattern of 90° SNWs [24,59], because a 90° SNW has only 12% of specific wall energy of the 180° SNW [20]. Such a transformation of the SNW into a CTW is observed in the simulated results in Fig. 2(b), as the angle of the SNW in Fig. 2(a) approaches to ~105°. A simplified schematic configuration of such a CTW is shown in Fig. 4(b) with an antivortex in the middle of the wall and one vortex on both right and left wall junction. In Fig. 1(b), the nucleation of two VAVPs creates two segments of reversed magnetization inside the domain wall, i.e., dark-brown to bright-brown color along the +y direction. One of the reversed wall segments between a vortex and an antivortex is marked by black markers in Fig. 1(b). The nucleation of the segments with reversed domain wall contrasts, i.e., the green to orange color along the +y direction, in the simulated results is shown in Fig. 2(b). Such reversed segments inside the domain wall enlarge with the further increase in the applied field along the −y direction, as indicated by the black markers in Figs. 1(b) to (e) in the MFM images, and seen in Figs. 2(b) to (d) in the simulated results. Upon increasing the field along the −y direction, the antivortices located at the cross-ties of the 90° SNWs stay more or less fixed at their nucleation sites [60,61], while the vortices displace towards the +x direction and annihilate with the next-neighboring antivortices rather than with the co-nucleated antivortices. The displacement of the vortex, which is formed at the left end of the SNW (location indicated by an arrow), towards the +x direction is shown in Figs. 1(b) to (e). The consequent reversal of the domain wall contrast as a result of the displacement of the vortex is

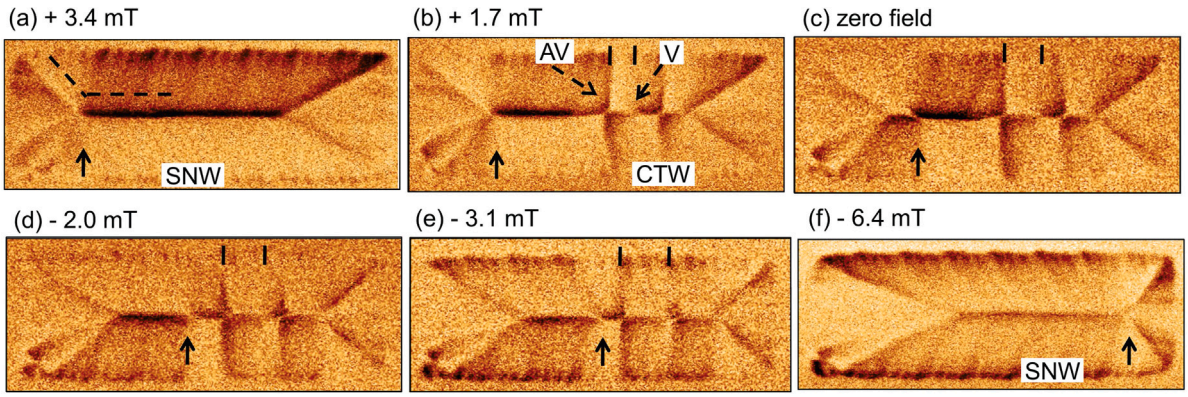

Fig. 1. MFM images of a 40 nm thick 2.3×6.7 μm^2 Py sample within different applied fields. A magnetic field was applied along the short axis of the sample, i.e., parallel to the y axis, and swept from +80 mT to −80 mT. (a) to (f) show the transformation steps of a SNW into a CTW and back to a SNW. The locations of a vortex (V) and an antivortex (AV) nucleated inside the CTW are shown in (b). Expansion of a reversed magnetization domain wall segment is described with black markers from (b) to (e). Black arrows display the displacement of a vortex inside the wall.

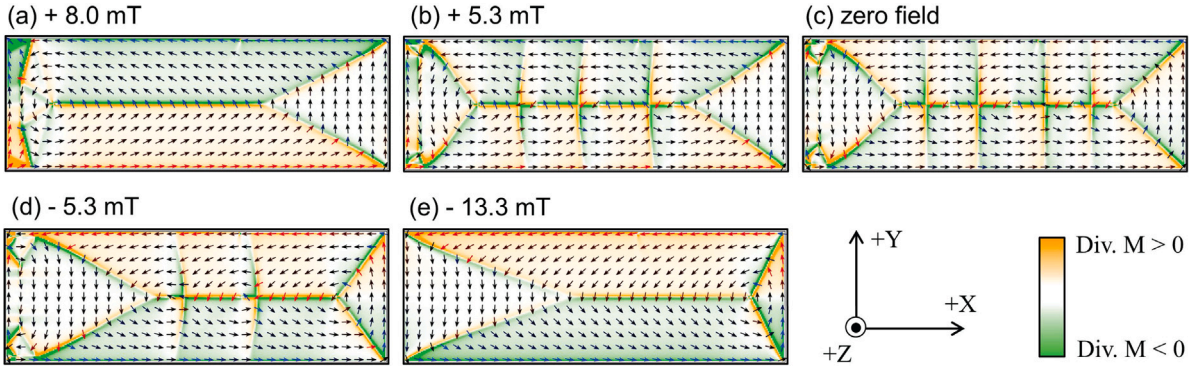

Fig. 2. OOMMF-simulated images of a 40 nm thick 2.3×6.7 μm^2 Py sample within different applied fields. A magnetic field was applied along the short axis of the sample, i.e., parallel to the y axis, and swept from +500 mT to −500 mT. Each arrow represents an averaged magnetization vector inside 11 × 11 adjacent cells at the sample surface. Black arrows are in-plane magnetization vectors, whereas blue and red arrows are the in-plane projections of the magnetization vectors tilted upwards and downwards, respectively. Green and orange areas represent positive and negative charge densities, respectively.

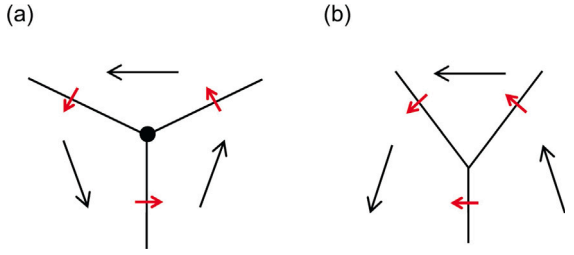

Fig. 3. Simplified schematics showing a domain wall junction (a) with and (b) without a vortex (shown as a dot) at the junction knot. Lines represent the domain walls. Magnetizations inside the domains and domain walls are represented by black and red arrows, respectively.

visible in these images. Displacements of all vortices towards the +x direction and their consequent annihilations with the corresponding next-neighboring antivortices lead to the reversal of the whole domain wall magnetization orientation from +y direction to −y direction. Finally, a SNW is again formed showing a continuous bipolar contrast with a single vortex attached at the right end of this domain wall, as shown in Figs. 1(f) and 2(e). Such a SNW with reversed magnetization is illustrated in Fig. 4(c). In this process, a resulting single vortex is displaced from one end of the SNW to another, via VAVPs nucleation and annihilation to reverse the domain wall magnetization.

4. Reversal of the internal magnetizations of two-dimensional domain walls

To interpret the surface magnetization of the sample observed by MFM measurements (Fig. 5), the domain configurations are visualized in different planes along the thickness of the sample (Fig. 6), as well as the cross-sections of the domain wall (Figs. 7 and 8) using three-dimensional micromagnetic simulations. To specify the different planes of views, the coordinate axes of the sample are selected as described in Fig. 6, where the scales along the x, y and z axes vary from 0 to 6700 nm, 0 to 2300 nm and 0 to 130 nm, respectively. For a general specification of the different viewing planes, the dimensions along all axes are converted into a dimensionless 0 to 1 scale. Fig. 5 shows the MFM data of the sample within different fields during the reversal of the sample' s magnetization parallel to the y axis (i.e., parallel to the short axis of the sample). The OOMMF-simulated images of the domain configurations in three different xy planes of the sample along the thickness, i.e., the lower plane (z = 0), middle plane (z = 0.5) and upper plane (z = 1.0) for different fields, are shown in Fig. 6. The locations of the vortices and antivortices are indicated in the upper and lower planes. The corresponding cross-sectional images of the domain wall in the yz planes at different field steps are presented in Figs. 7 and 8. In all cross-sectional images the out-of-plane direction towards the reader

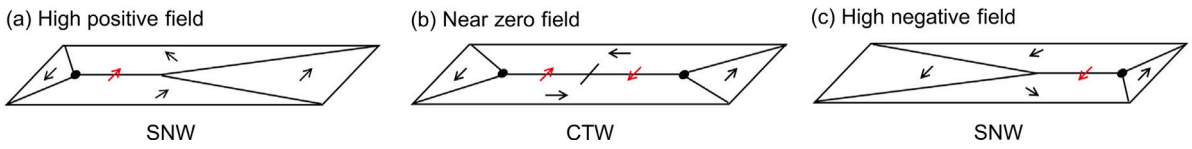

Fig. 4. Simplified schematics for magnetization inside the domains (black arrows) and domain walls (red arrows) in a 40 nm thick sample at different expected field range. Vortex is shown as a thick black dot.

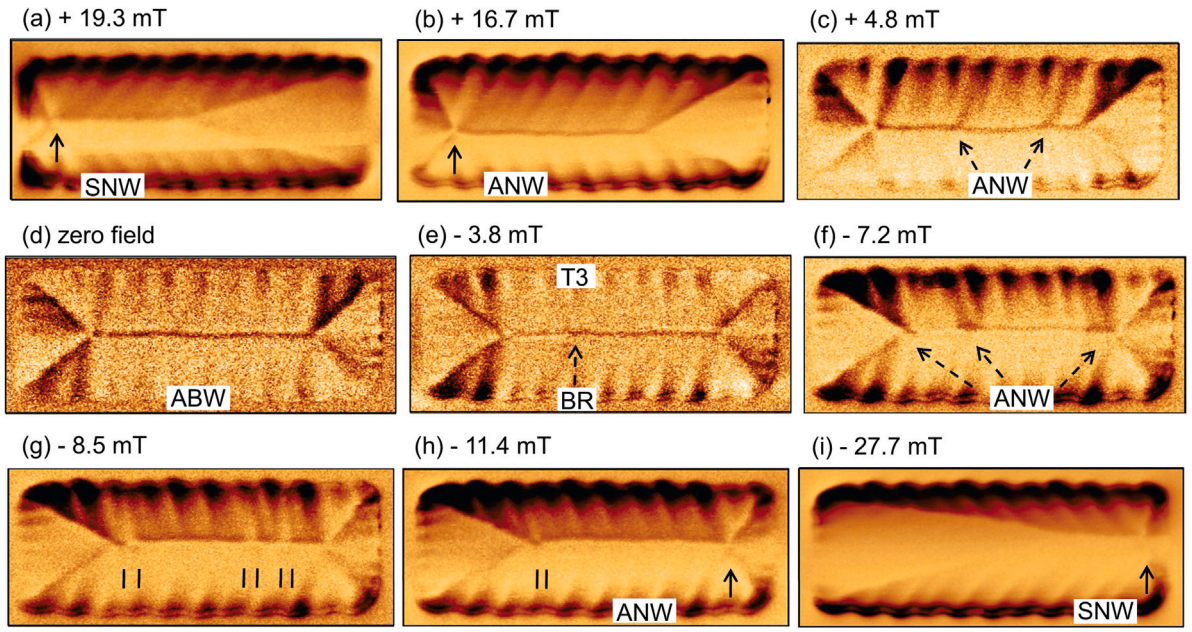

Fig. 5. MFM images of a 130 nm thick 2.3×6.7 μm^2 Py sample within different applied fields. A magnetic field was applied along the short axis of the sample and swept from +80 mT to −80 mT. (a) to (i) show the transformation steps of a SNW into an ADW and back to a SNW. In (e), the location of the reversal of the Bloch core, i.e., a Bloch reversal (BR), is indicated.

is along the +x direction. Also, simplified schematics of different types of domain walls are shown in Fig. 9.

The sample is first saturated along the +y direction. Upon decreasing the field to +19.3 mT, the domain walls formed along the long edges (not shown in the results) and join to form a single domain wall parallel to the x axis, as shown in Fig. 5(a). This domain wall is connected to two domain wall junctions at its ends (see Fig. 3 for wall junctions). This domain wall forms a bipolar contrast both in the MFM image in Fig. 5(a) and in the simulated result in Fig. 6(a). A continuous contrast of this wall along its length indicates the absence of any TS inside the wall. In Fig. 5(a), the domain wall forming the upper trapezoidal-shaped domain (as described before in Section 3) changes its contrast at the left domain wall junction. The contrast of this domain wall remains unchanged at the right domain wall junction. The reversal of the domain wall contrast at the left wall junction indicates the presence of a vortex at the left domain wall junction, which is also confirmed by comparing the MFM data in Fig. 5(a) with the simulated data in Fig. 6(a). The position of the vortex is marked by a black arrow in Fig. 5(a). A cross-sectional image of the wall taken from Fig. 6(a) is shown in Fig. 7(a). An in-plane orientation of the domain wall magnetization in the cross-sectional image in Fig. 7(a) and a bipolar contrast of this wall shown in Fig. 5(a) indicate that this domain wall is a SNW. The angle of this SNW is 80°, which was measured at the middle plane of Fig. 6(a). A schematic illustration of such a SNW is shown in Fig. 9(a). Upon further decreasing the applied field, the magnitude of the bipolar contrast of the domain wall in the MFM measurement decreases, as shown in Fig. 5(b). A cross-sectional view of the domain wall taken from the corresponding simulated image in Fig. 6(b) is shown in Fig. 7(b). From Fig. 6(b) it is found that the angle of this domain wall increases to 143°, and the magnetization configuration inside the domain wall transforms into a curved shape with the overall magnetization still pointing towards the +y direction, as observed in Fig. 7(b). With the decrease in the applied field, the magnetization inside adjacent domains relaxes more along the edges of the sample (i.e., parallel to the x axis), therefore, the angle of the domain wall increases. The increase in the domain wall angle leads to an increase in the magnetic charges around the wall [20]. However, the amount of the magnetic charges (formed due to the increasing angle) around a SNW configuration at this thickness (130 nm), would be much larger compared to the amount of the charges around the same angle SNW in a 40 nm thick sample. Therefore, with a decrease of the applied field, the one-dimensional SNW transforms into a curved shaped two-dimensional domain wall, instead of a cross-tie pattern of one-dimensional 90° SNWs (i.e., into a CTW as observed in the 40 nm thick sample). This domain wall is an ANW, where a partial out-of-plane magnetization orientation in the interior of the wall produces less magnetic charges around the wall, compared to the charges that would be produced around a same angle SNW. An ANW and the magnetization inside its adjacent domains are illustrated in the schematic diagram in Fig. 9(b). The bipolar nature of the MFM contrast of the ANW observed in Fig. 5(b) is because of the orientation of the overall magnetization inside the domain wall along +y direction [62,63]. Upon further reducing the applied field, the out-of-plane component of the magnetization in the interior of the domain wall increases to prevent the magnetic charges due to an increase in the wall angle. Therefore, the bipolar MFM contrast of the domain wall further reduces, as seen in Fig. 5(c). The cross-sectional view of the domain wall from Fig. 6(c) is shown in Fig. 7(c). With the further decrease of the applied field, the increase in the magnetic charges around the wall is prevented by transformation of the orientation of the overall magnetization along +z direction (shown

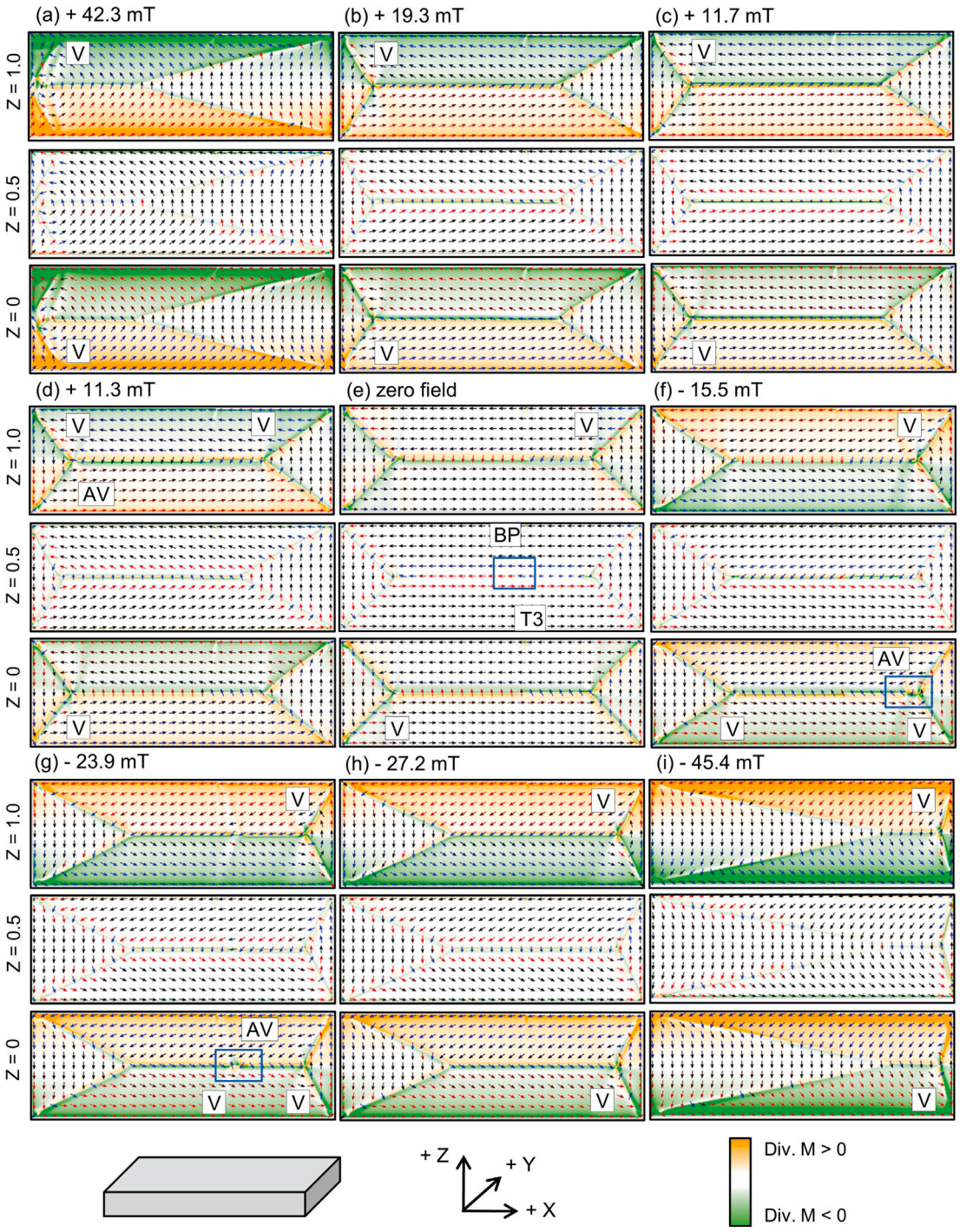

Fig. 6. OOMMF-simulated data for a 130 nm thick 2.3×6.7 μm^2 Py sample within different applied fields. A magnetic field was applied along the short axis of the sample and swept from +500 mT to −500 mT. Three images corresponding to three xy planes, i.e., z = 0, z = 0.5 and z = 1.0, along the thickness of the sample are shown for each magnetic field step. Positions of the vortex (V), antivortex (AV) and Bloch point (BP) are marked. Each arrow represents an averaged magnetization vector inside 11 × 11 adjacent cells. Black arrows are in-plane magnetization vectors, whereas blue and red arrows are the in-plane projection of magnetization vectors tilted upwards and downwards, respectively. Green and orange colored areas represent positive and negative charge densities, respectively.

in Fig. 7(d)). In this process, the magnetization in the interior of the domain wall rotates completely out of plane, and the domain wall transforms into an ABW with the reversal of one of the NCs at the sample surface. Such transitions of the ANW into an ABW are observed in the MFM measurements shown in Fig. 5(c), where the remaining ANW segments displaying slight bipolar contrasts are indicated by dashed arrows. In the upper plane (z = 1.0) presented in Fig. 6(d), a VAVP nucleates close to the right end of the domain wall. The antivortex, nucleated at the right end of the upper NC, moves towards the left end to reverse the upper NC and annihilates with the vortex present at the left end of the upper NC. The corresponding schematics is shown in Fig. 9(c). As antivortices at this thickness have no long "cross legs" (i.e., CTWs), they move easily. The cross-sectional image in Fig. 7(d) (taken at the same field as the xy planes shown in Fig. 6(d)) describes the reversal of the upper NC. The ANW to ABW transition stage in Fig. 5(c) displays the transformation of the bipolar contrast

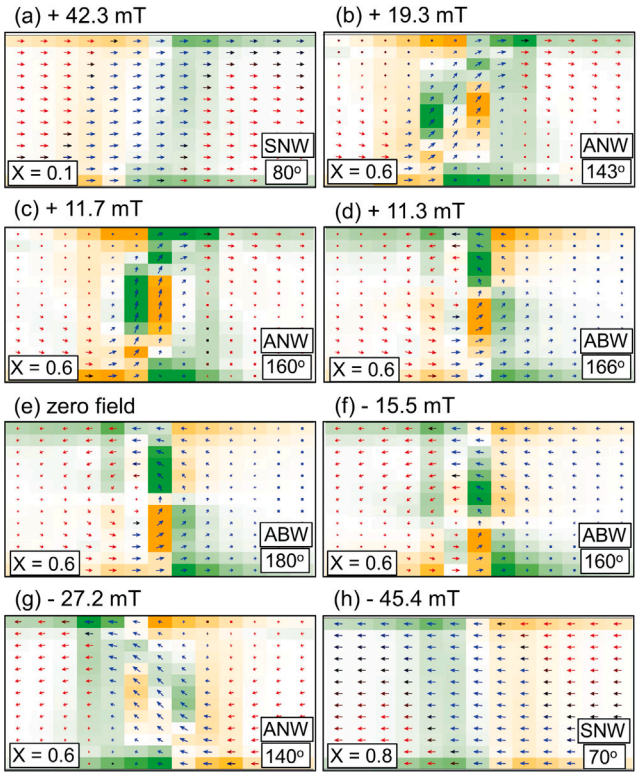

Fig. 7. Cross-sectional images of the domain wall along the yz planes taken from Fig. 6 within different applied fields. The x value in each image indicates the location parallel to the x axis at which the cross-sections are taken. The out-of-plane direction is along the +x direction. Domain wall angle is measured from the middle planes presented in Fig. 6. The images show a complete thickness of the sample i.e., 130 nm parallel to the z axis, while a 260 nm long segment of the sample parallel to the y axis is selected to describe the cross-sectional magnetization configuration of the domain wall. Each arrow represents an averaged magnetization vector inside a single cell. Black arrows represent the in-plane magnetization, whereas the red and blue colored arrows represent the out-of-plane projection of the magnetization inside a single cell. Green and orange colored areas represent positive and negative charge densities, respectively.

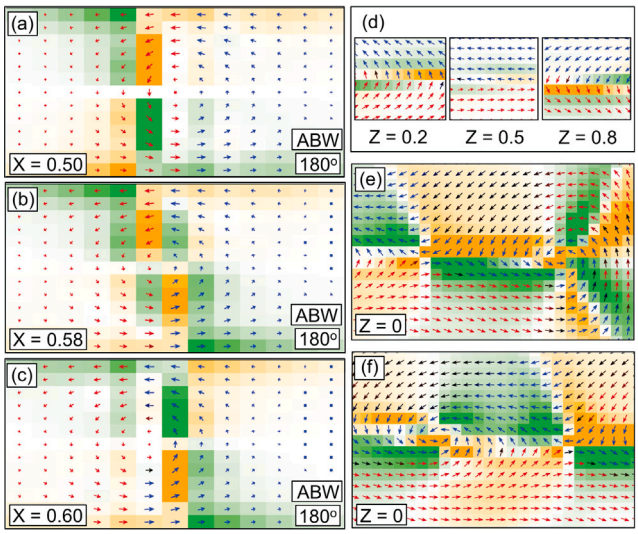

Fig. 8. (a) to (c) show the cross-sectional images of the "T3" TS inside the ABW at zero field in Fig. 6(e) from x = 0.5 to x = 0.6. The angle of the domain wall was measured from the middle plane in Fig. 6(e). (a) to (c) show the complete thickness of the sample i.e., 130 nm parallel to the z axis, while a 260 nm long segment of the sample parallel to the y axis is selected to describe the cross-sectional magnetization configuration of the domain wall. The magnetization configuration in the xy plane for this TS is shown in (d). (e) shows the magnetic configuration after the nucleation of a VAVP at the right end of the lower NC in Fig. 6(f). (f) shows the magnetic configuration before the VAVP annihilation at the lower NC in Fig. 6(g). Black arrows represent the in-plane magnetization, whereas red and blue ones represent the out-of-plane projection of the magnetization inside a single cell. Green and orange areas represent positive and negative charge densities, respectively.

to a unipolar contrast of the domain wall. Tiny segments of the bipolar contrast at locations close to the broken arrows indicate the presence of the TSs between the ANW and ABW segments of the domain wall. These TSs consist of vortices and antivortices inside the NCs at the locations of the transformations between the different types of ADWs (i.e., between ANWs and ABWs). At zero field, an ABW with a unipolar MFM contrast is formed as shown in Fig. 5(d), and in the simulated images in Figs. 6(e) and 7(e). The schematic orientation of an ABW is illustrated in Fig. 9(c). A transition between a clockwise and counter-clockwise ABW is observed by MFM in Fig. 5(e) and in the simulated data in Fig. 6(e). The magnetization configurations of the domain wall around this TS are shown in different cross-sectional yz planes in Figs. 8(a) to (c), and the configuration in different xy planes is shown in Fig. 8(d). This is a "T3" TS between the clockwise and counter-clockwise chiralities of the ABW [31,35,37,44]. The Bloch core of the ABW reverses its magnetization orientation, while the orientations of the NCs at both surfaces remains unreversed across this TS [31,35,37,44]. The Bloch reversal (BR) in the MFM data of Fig. 5(e) is observed with a reversal of the unipolar contrast of the ABW due to the reversal of the out-of-plane orientation between +z and −z directions. This TS contains a BP at its center [39,41–43]. The equal magnitude of the opposite out-of-plane orientations of the magnetization in Fig. 8(b) indicates the location of a BP in the "T3" TS in this simulated result. A further increase in the applied field along the −y direction starts saturating the domain wall magnetization in the reversed orientation. Therefore, the ABW which is favored only at small or zero fields [20,29] becomes unstable and transforms into an ANW with the reversal of the remaining NC, i.e., the lower NC. In Fig. 6(f), a VAVP nucleated in the lower NC ($Z = 0$) at the right end of the domain wall reverses a segment of the lower NC parallel to the direction of the applied field. The detailed magnetization configuration of this VAVP is shown in Fig. 8(e). Such reversals of NC segments and the consequent transformation of the ABW into an ANW are observed in Fig. 5(f). Three such segments of bipolar contrast domain walls nucleated inside the ABW are presented in Fig. 5(f). At this field, i.e. at −7.2 mT, ABWs and ANWs co-exist inside the domain wall. In Fig. 5(g), three VAVPs at the transitions between the ANW and ABW segments are indicated by black markers. In Figs. 6(g) (z = 0) and 8(f), one of such VAVP is shown inside the lower NC. Fig. 7(f) describes the onset of the lower NC reversal by pushing the cross-sectional vortex-like structure of the ABW towards the lower NC. VAVPs in Fig. 5(g) annihilate with an increase in the applied field, and the domain wall transforms into an ANW as shown in Figs. 5(h) and 6(h). The cross-sectional image in Fig. 7(g) (taken from Fig. 6(h)) shows an ANW with its overall magnetization pointing along the −y direction. The schematic illustration in Figs. 9(d) and (e) describe annihilation of vortex-antivortex pair in the lower NC and a resulting reversed ANW. Further increase of the magnetic field transforms the ANW into an SNW as shown in Figs. 5(i) and 6(i), which is clearly observed in the cross-sectional image in Fig. 7(h). A single vortex presents at the right end of this SNW is marked by a black arrow in Fig. 5(i), the presence of which is confirmed by the simulated data shown in Fig. 6(i). In this process, the magnetization throughout the domain wall rotates again in the in-plane orientation. A reduced angle of the domain wall, i.e., 70° in Fig. 7(h), at a high magnetic field strength keeps the magnetic charges low around the domain wall. A reversed SNW is illustrated in Fig. 9(f).

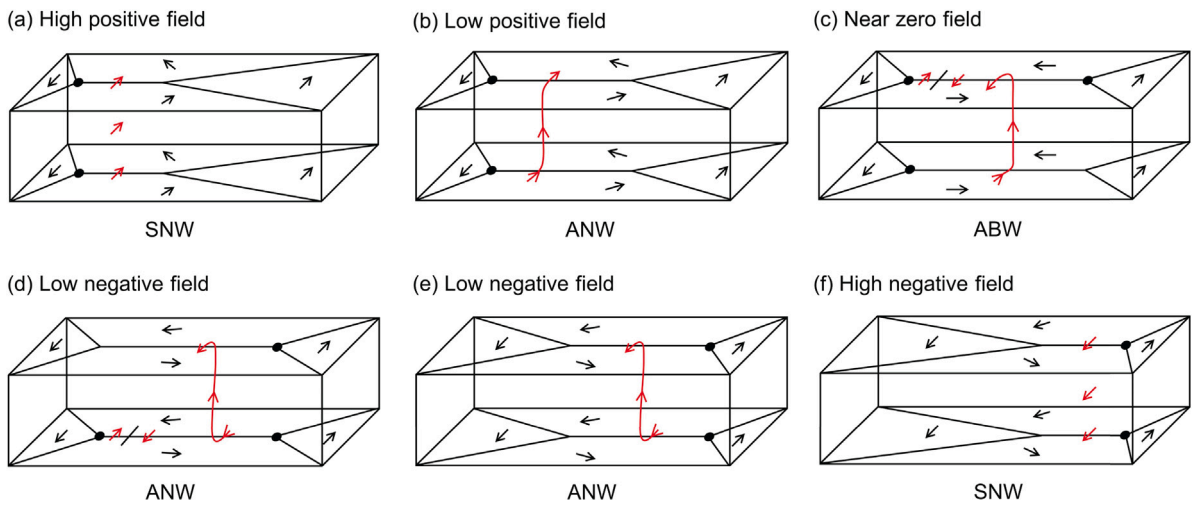

Fig. 9. Simplified schematics for magnetization inside the domains (black arrows) and domain walls (red arrows) in a 130 nm thick sample at different expected field range. Vortex is shown as a thick black dot.

The spike-shaped contrast formed at the sample edges in Fig. 5 is due to the magnetic charges appearing at the imperfect edges of the sample. This contrast is absent in the simulated images shown in Fig. 6 due to the assumption of perfect edges of the sample. Rough boundaries can lead to the pinning of domain walls and hence can change the remanent state during magnetization reversals [23,64]. The focus of this study is to discuss the reversal of one- and two-dimensional domain walls, which formed along the long axis of the structures. The spike-shaped contrast had no influence on the reversal of these domain wall, which was proved in the simulations. However, the number of vortices and antivortices within the domain walls can vary with the magnetic anisotropy and pinning sites within the material body. More specifically, the number of vortices and antivortices can change with the composition of material, thickness and grannular structure of the film [23]. All this could lead to a change of number of nucleations and annihilations of vortices and antivortices within the domain walls. At least one vortex-antivortex nucleation and annihilation event is required to switch the NCs of the two-dimensional domain walls or the SNWs in one-dimensional domain walls. However, in particular the basic mechanism of domain wall reversal (by changing the shape and types of domain walls) would remain the same.

Recent investigations on the domain wall dynamics have advanced the control and manipulation of domain walls [65,66]. For example, Jeon et al. [67] have shown that the spacing between chiral domain walls can be controlled down to sub−100 nm and Guan et al. [68] presented that using ionic liquid gating the domain wall speed can reach several hundred ms^{-1}. We investigated the two-dimensional domain walls in a static field. In a dynamic field, the behavior of the vortices, antivortices and singularities would play a crucial role in determining the stability and motion of two-dimensional domain walls.

5. Conclusion

The role of vortices and antivortices as TSs in the reversal of the internal magnetization of one-dimensional and two-dimensional domain walls is explained. TSs nucleate and annihilate to stabilize the domain walls against the magnetic charges induced inside a varying magnetic field. Segments of domain walls with reversed magnetization orientations nucleate and enlarge with the nucleation and annihilation of TSs, respectively. In this process, domain walls complete the reversal of their magnetization configurations by displacing a resulting single vortex along their axes. However, with the change of the film thickness, the different modes of transformations inside the domain walls lead to a change in the behavior of the TSs.

In 40 nm thick films, the domain walls reverse their magnetization configurations through in-plane rotations of their magnetizations. Nucleation of vortices and antivortices as the TSs inside one-dimensional domain walls reduces the magnetic charges by transforming the domain walls into the segments of smaller-angle domain walls. This results in the transformation of a SNW into a CTW. The CTW transforms back into a SNW with reversed magnetization orientations to complete the domain walls' magnetization reversal.

The domain walls in 130 nm thick films reverse their magnetization configurations through both in-plane and out-of-plane rotations of their magnetizations. First, an out-of-plane rotation of magnetization in the interior of the domain walls transforms the one-dimensional SNWs into two-dimensional ANWs. Thereafter, the two-dimensional ANWs reverse their magnetization by the in-plane reversal of both of their NCs' magnetization configurations, with the nucleation of vortices and antivortices inside the NCs. This reversal of the two-dimensional ANWs' magnetization configurations proceeds via their transformations into two-dimensional ABWs. Finally, the reversed two-dimensional ANWs transform into reversed one-dimensional SNWs by another out-of-plane rotation of magnetization. Reversal of the internal magnetizations of the walls at this thickness proceed through successive reversal of upper and lower NCs, or vice versa, which generates three-dimensional TSs. The TSs at this thickness stabilize the domain walls by changing the shapes of the walls (i.e., by changing ANWs into ABWs), rather than transforming the domain walls into smaller-angle wall-segments.

Since flux closure magnetizations are also formed in soft magnetic materials other than Py [20]. The domain wall reversal mechanism described in the manuscript is also valid for other soft magnetic materials [20,69]. However, the thicknesses of the materials for the formation of one- and two-dimensional domain walls could vary.

CRediT authorship contribution statement

Sukhvinder Singh: Writing – original draft, Visualization, Methodology, Investigation, Formal analysis, Data curation, Conceptualization. **Haibin Gao:** Writing – review & editing, Supervision. **Uwe Hartmann:** Writing – review & editing, Validation, Supervision, Resources, Project administration, Conceptualization.

Declaration of competing interest

The authors declare that they have no known competing financial interests or personal relationships that could have appeared to influence the work reported in this paper.

Data availability

Data will be made available on request.

References

[1] D. Giuliano, L. Gnoli, V. Ahrens, M.R. Roch, M. Becherer, G. Turvani, M. Vacca, F. Riente, Ga^+ ion irradiation-induced tuning of artificial pinning sites to control domain wall motion, ACS Appl. Electron. Mater. 5 (2) (2023) 985–993, http://dx.doi.org/10.1021/acsaelm.2c01510.

[2] F. Cheynis, A. Masseboeuf, O. Fruchart, N. Rougemaille, J.C. Toussaint, R. Belkhou, P. Bayle-Guillemaud, A. Marty, Controlled switching of néel caps in flux-closure magnetic dots, Phys. Rev. Lett. 102 (10) (2009) 107201, http://dx.doi.org/10.1103/PhysRevLett.102.107201.

[3] O. Fruchart, N. Rougemaille, A. Bendounan, J.-C. Toussaint, R. Belkhou, Yuan Tian, Hyeonseung Yu, F. Cheynis, A. Masseboeuf, P. Bayle-Guillemaud, A. Marty, Asymmetric hysteresis of néel caps in flux-closure magnetic dots, IEEE Trans. Magn. 46 (6) (2010) 1552–1555, http://dx.doi.org/10.1109/TMAG.2010.2043222.

[4] V.D. Nguyen, O. Fruchart, S. Pizzini, J. Vogel, J.-C. Toussaint, N. Rougemaille, Third type of domain wall in soft magnetic nanostrips, Sci. Rep. 5 (2015) 12417, http://dx.doi.org/10.1038/srep12417.

[5] A. Arrott, R. Hertel, Large amplitude oscillations (switching) of bi-stable vortex structures in zero field, J. Magn. Magn. Mater. 322 (9–12) (2010) 1389–1391, http://dx.doi.org/10.1016/j.jmmm.2009.04.083.

[6] C. Zinoni, A. Vanhaverbeke, P. Eib, G. Salis, R. Allenspach, Beyond the compact magnetic domain wall, Phys. Rev. Lett. 107 (20) (2011) 207204, http://dx.doi.org/10.1103/PhysRevLett.107.207204.

[7] S.K. Karna, M. Marshall, W. Xie, L. DeBeer-Schmitt, D.P. Young, I. Vekhter, W.A. Shelton, A. Kovács, M. Charilaou, J.F. DiTusa, Annihilation and control of chiral domain walls with magnetic fields, Nano Lett. 21 (3) (2021) 1205–1212, http://dx.doi.org/10.1021/acs.nanolett.0c03199.

[8] R.M. Vakhitov, R.V. Solonetsky, V.R. Gurjanova, A.R. Nizjamova, D.A. Sechin, T.T. Gareev, A.P. Pyatakov, Magnetic-field tuning of domain-wall multiferroicity, Phys. Rev. B 104 (2021) 144407, http://dx.doi.org/10.1103/PhysRevB.104.144407.

[9] H.-S. Han, S. Lee, M.-S. Jung, N. Kim, W. Chao, Y.-S. Yu, J.-I. Hong, K.-S. Lee, M.-Y. Im, Topology-dependent stability of vortex-antivortex structures, Appl. Phys. Lett. 118 (21) (2021) 212407, http://dx.doi.org/10.1063/5.0045593.

[10] L. Huang, Y. Zhu, Controlled reversal of coupled Néel walls in flux-closure magnetic trilayer elements, Appl. Phys. Lett. 95 (22) (2009) 10–13, http://dx.doi.org/10.1063/1.3269608.

[11] S.S.P. Parkin, M. Hayashi, L. Thomas, Magnetic domain-wall racetrack memory, Science 320 (5873) (2008) 190–194, http://dx.doi.org/10.1126/science.1145799.

[12] E. Raymenants, D. Wan, S. Couet, Y. Canvel, A. Thiam, D. Tsvetanova, L. Souriau, I. Asselberghs, R. Carpenter, N. Jossart, M. Manfrini, A. Vaysset, O. Bultynck, S. Van Beek, M. Heyns, D. Nikonov, I. Young, S. Ghosh, L. Vila, K. Garello, S. Pizzini, V. Nguyen, I. Radu, Magnetic domain walls: from physics to devices, IEDM, in: 2021 IEEE International Electron Devices Meeting, vol. 2021-Decem, IEEE, Raymenants2021, 2021, pp. 32.3.1–32.3.4, http://dx.doi.org/10.1109/IEDM19574.2021.9720689.

[13] P. Pirro, T. Koyama, T. Brächer, T. Sebastian, B. Leven, B. Hillebrands, Experimental observation of the interaction of propagating spin waves with Néel domain walls in a Landau domain structure, Appl. Phys. Lett. 106 (23) (2015) 232405, http://dx.doi.org/10.1063/1.4922396.

[14] K. Wagner, A. Kákay, K. Schultheiss, A. Henschke, T. Sebastian, H. Schultheiss, Magnetic domain walls as reconfigurable spin-wave nanochannels, Nat. Nanotechnol. 11 (5) (2016) 432–436, http://dx.doi.org/10.1038/nnano.2015.339.

[15] F. Garcia-Sanchez, P. Borys, R. Soucaille, J.-p. Adam, R.L. Stamps, J.-v. Kim, Narrow magnonic waveguides based on domain walls, Phys. Rev. Lett. 114 (24) (2015) 247206, http://dx.doi.org/10.1103/PhysRevLett.114.247206.

[16] J. Lan, W. Yu, J. Xiao, Geometric magnonics with chiral magnetic domain walls, Phys. Rev. B 103 (2021) 214407, http://dx.doi.org/10.1103/PhysRevB.103.214407.

[17] S. Zhang, A.A. Baker, S. Komineas, T. Hesjedal, Topological computation based on direct magnetic logic communication, Sci. Rep. 5 (2015) 15773, http://dx.doi.org/10.1038/srep15773.

[18] H.-S. Han, S. Lee, M.-S. Jung, N. Kim, D.-H. Jung, M. Kang, H.-J. Ok, W. Chao, Y.-S. Yu, J.-I. Hong, M.-Y. Im, K.-S. Lee, Tuning of oscillation modes by controlling dimensionality of spin structures, NPG Asia Mater. 14 (2022) 91, http://dx.doi.org/10.1038/s41427-022-00438-9.

[19] Q.L. He, T.L. Hughes, N.P. Armitage, Y. Tokura, K.L. Wang, Topological spintronics and magnetoelectronics, Nat. Mater. 21 (2022) 15–23, http://dx.doi.org/10.1038/s41563-021-01138-5.

[20] A. Hubert, R. Schäfer, Magnetic Domains : the Analysis of Magnetic Microstructures, Springer, Berlin, 1998.

[21] S. Singh, H. Gao, U. Hartmann, Nucleation of stripe domains in thin ferromagnetic films, Phys. Rev. B 98 (2018) 060414, http://dx.doi.org/10.1103/PhysRevB.98.060414.

[22] S. Voltan, C. Cirillo, H.J. Snijders, K. Lahabi, A. García-Santiago, J.M. Hernández, C. Attanasio, J. Aarts, Emergence of the stripe-domain phase in patterned permalloy films, Phys. Rev. B 94 (9) (2016) 094406, http://dx.doi.org/10.1103/PhysRevB.94.094406.

[23] S. Singh, L. Abelmann, H. Gao, U. Hartmann, Influence of sputter pressure on magnetic and structural properties of permalloy thin films, J. Magn. Magn. Mater. 586 (2023) 171138, http://dx.doi.org/10.1016/j.jmmm.2023.171138.

[24] A. Hubert, Domain wall structures in thin magnetic films, IEEE Trans. Magn. 11 (5) (1975) 1285–1290, http://dx.doi.org/10.1109/TMAG.1975.1058830.

[25] N. Wiese, S. McVitie, J.N. Chapman, A. Capella-Kort, F. Otto, On the scaling behaviour of cross-tie domain wall structures in patterned NiFe elements, EPL 80 (5) (2007) 57003, http://dx.doi.org/10.1209/0295-5075/80/57003.

[26] M.J. Donahue, Micromagnetic investigation of periodic cross-tie/vortex wall geometry, Adv. Cond. Matter Phys. 2012 (4) (2012) 1–8, http://dx.doi.org/10.1155/2012/908692.

[27] A. Hubert, Stray-field-free magnetization configurations, Phys. Status Solidi (B) 32 (2) (1969) 519–534, http://dx.doi.org/10.1002/pssb.19690320204.

[28] W. Rave, A. Hubert, Micromagnetic calculation of the thickness dependence of surface and interior width of asymmetrical Bloch walls, J. Magn. Magn. Mater. 184 (2) (1998) 179–183, http://dx.doi.org/10.1016/S0304-8853(97)01126-8.

[29] A. Hubert, Domain wall phenomena in bubble propagation layers, J. Magn. Magn. Mater. 35 (1) (1983) 249–253, http://dx.doi.org/10.1016/0304-8853(83)90510-3.

[30] T. Herranen, L. Laurson, Barkhausen noise from precessional domain wall motion, Phys. Rev. Lett. 122 (2019) 117205, http://dx.doi.org/10.1103/PhysRevLett.122.117205.

[31] V.V. Zverev, B.N. Filippov, Transition micromagnetic structures in asymmetric vortexlike domain walls (static solutions and dynamic reconstructions), J. Exp. Theor. Phys. 117 (1) (2013) 108–120, http://dx.doi.org/10.1134/S1063776113080219.

[32] V.V. Zverev, B.N. Filippov, Simulation of three-dimensional micromagnetic structures in magnetically uniaxial films with in-plane anisotropy. Dynamics and structural reconstructions, Phys. Met. Met. 114 (2) (2013) 116–121, http://dx.doi.org/10.1134/S0031918X13020154.

[33] S. Huo, J. Bishop, J. Tucker, W. Rainforth, H. Davies, 3-d simulation of Bloch lines in 180° domain walls in thin iron films, J. Magn. Magn. Mater. 177–181 (Part 1) (1998) 229–230, http://dx.doi.org/10.1016/S0304-8853(97)00670-7.

[34] M.N. Dubovic, V.V. Zverev, B.N. Filippov, Nonlinear rearrangement of the structure of domain walls in a thin magnetic film with a uniaxial in-plane anisotropy, Phys. Met. Met. 115 (11) (2014) 1160–1177, http://dx.doi.org/10.1134/S0031918X14110027.

[35] H. Asada, H. Kubo, J. Yamasaki, M. Takezawa, T. Koyanagi, Micromagnetic simulation of wall transition structures with self-induced helical anisotropy and their pinning effects, J. Phys.: Conf. Ser. 200 (4) (2010) 042003, http://dx.doi.org/10.1088/1742-6596/200/4/042003.

[36] M. Redjdal, A. Kakay, T. Trunk, M.F. Ruane, F.B. Humphrey, Simulation of three-dimensional nonperiodic structures of π-vertical Bloch line (pi-VBL) and 2π-VBL (2pi-VBL) in permalloy films, J. Appl. Phys. 89 (11) (2001) 7609, http://dx.doi.org/10.1063/1.1355351.

[37] M. Schneider, S. Müller-Pfeiffer, W. Zinn, Magnetic force microscopy of domain wall fine structures in iron films, J. Appl. Phys. 79 (11) (1996) 8578, http://dx.doi.org/10.1063/1.362539.

[38] S. Huo, J. Bishop, J. Tucker, W. Rainforth, H. Davies, 3-D micromagnetic simulation of a Bloch line between C-sections of a 180° domain wall in a {100} iron film, J. Magn. Magn. Mater. 218 (1) (2000) 103–113, http://dx.doi.org/10.1016/S0304-8853(00)00365-6.

[39] V.V. Zverev, B.N. Filippov, M.N. Dubovik, Transition micromagnetic structures in the Bloch and Néel asymmetric domain walls containing singular points, Phys. Solid State 56 (9) (2014) 1785–1794, http://dx.doi.org/10.1134/S1063783414090327.

[40] B. Filippov, M. Dubovik, V. Zverev, Numerical studies of micromagnetic configurations in stripes with in-plane anisotropy and low quality factor, J. Magn. Magn. Mater. 374 (2015) 600–606, http://dx.doi.org/10.1016/j.jmmm.2014.09.011.

[41] R.G. Elías, A. Verga, Magnetization structure of a Bloch point singularity, Eur. Phys. J. B 82 (2) (2011) 159–166, http://dx.doi.org/10.1140/epjb/e2011-20146-6.

[42] A. Masseboeuf, T. Jourdan, F. Lançon, P. Bayle-Guillemaud, A. Marty, Probing magnetic singularities during magnetization process in FePd films, Appl. Phys. Lett. 95 (21) (2009) 212501, http://dx.doi.org/10.1063/1.3266825.

[43] A. Thiaville, J.M. Garćia, R. Dittrich, J. Miltat, T. Schrefl, Micromagnetic study of Bloch-point-mediated vortex core reversal, Phys. Rev. B 67 (2003) 094410, http://dx.doi.org/10.1103/PhysRevB.67.094410.

[44] M.-Y. Im, H.-S. Han, M.-S. Jung, Y.-S. Yu, S. Lee, S. Yoon, W. Chao, P. Fischer, J.-I. Hong, K.-S. Lee, Dynamics of the Bloch point in an asymmetric permalloy disk, Nat. Commun. 10 (2019) 593, http://dx.doi.org/10.1038/s41467-019-08327-6.

[45] S.S.P.K. Arekapudi, B. Böhm, L. Ramasubramanian, F. Ganss, P. Heinig, S. Stienen, C. Fowley, K. Lenz, A.M. Deac, M. Albrecht, O. Hellwig, Direct imaging of distorted vortex structures and magnetic vortex annihilation processes in ferromagnetic/antiferromagnetic disk structures, Phys. Rev. B 103 (2021) 014405, http://dx.doi.org/10.1103/PhysRevB.103.014405.

[46] J. Hermosa, A. Hierro-Rodríguez, C. Quirós, J.I. Martín, A. Sorrentino, L. Aballe, E. Pereiro, M. Vélez, S. Ferrer, Bloch points and topological dipoles observed by X-ray vector magnetic tomography in a ferromagnetic microstructure, Commun. Phys. 6 (2023) 49, http://dx.doi.org/10.1038/s42005-023-01162-8.

[47] M. Redjdal, A. Kákay, M.F. Ruane, F.B. Humphrey, Magnetic domain wall transitions based on chirality change and vortex position in thin permalloy™ films, J. Appl. Phys. 91 (10) (2002) 8278, http://dx.doi.org/10.1063/1.1454983.

[48] B.N. Filippov, M.N. Dubovik, Influence of three-dimensional inhomogeneities of the magnetic parameters on the dynamics of vortex-like domain walls, Phys. Solid State 56 (5) (2014) 967–974, http://dx.doi.org/10.1134/S1063783414050084.

[49] A. Hubert, Stray-field-free and related domain wall configurations in thin magnetic films (II), Phys. Status Solidi 38 (2) (1970) 699–713, http://dx.doi.org/10.1002/pssb.19700380221.

[50] J. Miltat, A. Thiaville, P. Trouilloud, Néel lines structures and energies in uniaxial ferromagnets with quality factor Q > 1, J. Magn. Magn. Mater. 82 (2–3) (1989) 297–308, http://dx.doi.org/10.1016/0304-8853(89)90169-8.

[51] K. Babcock, V. Elings, M. Dugas, S. Loper, Optimization of thin-film tips for magnetic force microscopy, IEEE Trans. Magn. 30 (6) (1994) 4503–4505, http://dx.doi.org/10.1109/20.334130.

[52] M.J. Donahue, D.G. Porter, OOMMF User's Guide, Version 1.0, NISTIR 6376, National Institute of Standards and Technology, Gaithersburg, MD, 1999.

[53] D.V. Berkov, K. Ramstöcck, A. Hubert, Solving micromagnetic problems. Towards an optimal numerical method, Phys. Status Solidi A 137 (1) (1993) 207–225, http://dx.doi.org/10.1002/pssa.2211370118.

[54] D.A. Garanin, Fokker-Planck and Landau-Lifshitz-Bloch equations for classical ferromagnets, Phys. Rev. B 55 (1997) 3050–3057, http://dx.doi.org/10.1103/PhysRevB.55.3050.

[55] J. Steiner, R. Schäfer, H. Wieczoreck, J. McCord, F. Otto, Formation and coarsening of the concertina magnetization pattern in elongated thin-film elements, Phys. Rev. B 85 (10) (2012) 104407, http://dx.doi.org/10.1103/PhysRevB.85.104407.

[56] H.A.M. Van Den Berg, Domain structures in soft-ferromagnetic thin-film objects (invited), J. Appl. Phys. 61 (8) (1987) 4194–4199, http://dx.doi.org/10.1063/1.338474.

[57] H.A.M. Van Den Berg, D.K. Vatvani, Wall clusters and domain structure conversions, IEEE Trans. Magn. 18 (3) (1982) 880–887, http://dx.doi.org/10.1109/TMAG.1982.1061919.

[58] D. Rugar, H.J. Mamin, P. Guethner, S.E. Lambert, J.E. Stern, I. McFadyen, T. Yogi, Magnetic force microscopy: General principles and application to longitudinal recording media, J. Appl. Phys. 68 (3) (1990) 1169–1183, http://dx.doi.org/10.1063/1.346713.

[59] S. Middelhoek, Domain walls in thin NiFe films, J. Appl. Phys. 34 (4) (1963) 1054–1059, http://dx.doi.org/10.1063/1.1729367.

[60] R.D. Gomez, J.S. Ma, A. Arkilic, S.H. Chung, C. Krafft, Vortex-antivortex creation and annihilation on CoFeB crosstie patterns, J. Appl. Phys. 109 (7) (2011) 07D310, http://dx.doi.org/10.1063/1.3536342.

[61] F. Kloodt-Twesten, S. Kuhrau, P. Staeck, D.R. Cavicchia, F. Lofink, H.P. Oepen, R. Frömter, Coupling between vortices and antivortices in a cross-tie wall studied by time-resolved SEMPA, Phys. Rev. B 97 (2018) 024426, http://dx.doi.org/10.1103/PhysRevB.97.024426.

[62] S. Huo, J. Bishop, J. Tucker, W. Rainforth, H. Davies, Modelling of MFM images of 180° and 90° domain walls in iron films, IEEE Trans. Magn. 33 (5) (1997) 4056–4058, http://dx.doi.org/10.1109/20.619661.

[63] S. Müller-Pfeiffer, M. Schneider, W. Zinn, Imaging of magnetic domain walls in iron with a magnetic force microscope: A numerical study, Phys. Rev. B 49 (22) (1994) 15745–15752, http://dx.doi.org/10.1103/PhysRevB.49.15745.

[64] M.T. Bryan, D. Atkinson, R.P. Cowburn, Experimental study of the influence of edge roughness on magnetization switching in permalloy nanostructures, Appl. Phys. Lett. 85 (16) (2004) 3510–3512, http://dx.doi.org/10.1063/1.1806566.

[65] D. Kumar, T. Jin, R. Sbiaa, M. Kläui, S. Bedanta, S. Fukami, D. Ravelosona, S.-H. Yang, X. Liu, S. Piramanayagam, Domain wall memory: Physics, materials, and devices, Phys. Rep. 958 (2022) 1–35, http://dx.doi.org/10.1016/j.physrep.2022.02.001.

[66] G. Venkat, D.A. Allwood, T.J. Hayward, Magnetic domain walls: types, processes and applications, J. Phys. D: Appl. Phys. 57 (6) (2023) 063001, http://dx.doi.org/10.1088/1361-6463/ad0568.

[67] J.C. Jeon, A. Migliorini, L. Fischer, J. Yoon, S.S. Parkin, Dynamic manipulation of chiral domain wall spacing for advanced spintronic memory and logic devices, ACS Nano 18 (2024) 14507–14513, http://dx.doi.org/10.1021/acsnano.4c02024.

[68] Y. Guan, X. Zhou, F. Li, T. Ma, S.-H. Yang, S.S.P. Parkin, Ionitronic manipulation of current-induced domain wall motion in synthetic antiferromagnets, Nat. Commun. 12 (2021) 5002, http://dx.doi.org/10.1038/s41467-021-25292-1.

[69] A. Holz, H. Kronmüller, The nucleation of stripe domains in thin ferromagnetic films, Phys. Status Solidi 31 (2) (1969) 787–798, http://dx.doi.org/10.1002/pssb.19690310238.